

The use of astronomy VLBA campaign MOJAVE for geodesy

Hana Krásná · Leonid Petrov

Received: 02 May 2021 / Accepted: date

Abstract We investigated the suitability of the astronomical 15 GHz VLBA observing program MOJAVE-5 for estimation of geodetic parameters, such as station coordinates and Earth orientation parameters. We processed contemporary geodetic dual-band RV and CN experiments observed at 2.3 GHz and 8.6 GHz starting on September 2016 through July 2020 as reference dataset. We showed that the baseline length repeatability from MOJAVE-5 experiments is only a factor of 1.5 greater than from the dedicated geodetic dataset and still below 1 ppb. The wrms of the difference of estimated EOP with respect to the reference IERS C04 time series are a factor of 1.3 to 1.8 worse. We isolated three major differences between the datasets in terms their possible impact on the geodetic results, i.e. the scheduling approach, treatment of the ionospheric delay, and selection of target radio sources. We showed that the major factor causing discrepancies in the estimated geodetic parameters is the different scheduling approach of the datasets. We conclude that systematic errors in MOJAVE-5 dataset are low enough for these data to be used as an excellent testbed for further investigations on the radio source structure effects in geodesy and astrometry.

Keywords VLBA · MOJAVE · TRF · EOP

H. Krásná

1. Department of Geodesy and Geoinformation, Technische Universität Wien, Vienna, Austria

2. Astronomical Institute of the Czech Academy of Sciences, Prague, Czech Republic

E-mail: hana.krasna@tuwien.ac.at

L. Petrov

NASA Goddard Space Flight Center, Code 61A, Greenbelt, USA

1 Introduction

Group delay of an extended source observed with very long baseline interferometry (VLBI) differs from the group delay of a point source. Up to now, the contribution of source structure is not included in routine analysis of VLBI data. It was known for long time that source structure is a significant (e.g., Zeppenfeld, 1993; Sovers et al., 2002; Tornatore and Charlot, 2007; Shabala et al., 2015; Petrov and Kovalev, 2017) or even the major (Anderson and Xu, 2018) contributor to the error budget in geodetic VLBI.

One of the most promising ways to compute the source structure contribution to group delay is to generate images from the same VLBI observations, perform their 2D Fourier transform over spatial coordinates, and use it for calculation of structure delay (see, e.g., Petrov and Kovalev, 2017). Unfortunately, geodetic observing schedules are not well suited for producing good quality images. A typical geodetic schedule splits the network into a number of ad hoc subarrays, so a subset of stations observes one source and a subset of other stations observes another source at the same time, and upon completion of integration another subset of stations observes the next source. This leads to a substantial reduction of the number of closures in phase and amplitude required for robust imaging. Astronomical schedules usually avoid subarrays. The use of data for geodesy and astrometry from astronomical programs designed for imaging was not common in the past because four to eight intermediate recorded frequencies (IFs) were usually allocated contiguously, while for geodetic applications the frequencies are allocated as wide as possible. As a result, group delay uncertainty at a given signal to noise ratio (SNR) was an order of magnitude worse than from geodetic sched-

ules. Although such data were still useful for astrometry (Petrov, 2011, 2013), they were too coarse for precise geodesy. A non-contiguous allocation of intermediate frequencies for astronomy projects was rare because usually it was not required, and a commonly used AIPS software package (Greisen, 2003) that implemented the fringe fitting procedure does not support direct processing of such data. In a case when a goal of astronomical observation requires wide spanned bandwidth, e.g., for VLBA (Very Long Baseline Array) Imaging and Polarimetry Survey at 5 GHz (Helmboldt et al., 2007), processing astronomical data in a geodetic/astrometric mode was feasible and provided good results (Petrov and Taylor, 2011). However, single-band observations at rather low frequencies such as 5 GHz are affected by the ionospheric contribution, and this limits their usability for geodesy.

Progress in radioastronomy instrumentation resulted in an increase of recorded bandwidth. Since 2016–2020 astronomical observations typically cover a frequency band of 256 or 512 MHz. Group delay precision from these setups is close to the precision reached at geodetic setups. Therefore, the use of astronomical observing program seems feasible as a testbed for studying source structure contribution in detail provided that such a program satisfies two other remaining criteria: a) it observes strong sources and b) it is conducted at rather high frequencies to minimize the impact of the ionosphere. MOJAVE-5 (Monitoring Of Jets in Active galactic nuclei with VLBA Experiments) suits both these criteria. The program started in 1994 (Lister et al., 2018) and is focused on observations of bright active galactic nuclei (AGNs) with discernible structure at 15 GHz.

2 Motivation

Before commencing a thorough investigation of the impact of source structure on astrometry and geodesy results, we need establish a solid foundation of that work. MOJAVE-5 dataset differs from an usual geodetic dataset a) by the way how it was scheduled; b) by observing frequencies; and c) by the source selection.

An observing schedule consists of a sequence of time intervals called scans when all or a part of antennas of the network record voltage from a given source. Astronomical schedules are usually made by optimization of the uv -coverage, i.e. projections of the baseline vector on the plane tangential to the source direction. The scheduling goal of astronomical experiments is to generate such a sequence of observations that covers that plane as uniform as possible for each program source.

Geodetic schedules are usually designed to optimize elevation/azimuth coverage at each station for short time intervals (1–3 hours).

Geodetic observations are done at two or more frequencies simultaneously. Since the ionospheric group delay is frequency dependent, multi-band observations allow to derive an ionosphere free combination of group delays. Astronomical observations are usually done at one frequency at once. Therefore, group delay observables from astronomical observations are affected by the ionosphere.

A list of ~ 100 objects is usually observed with geodesy schedules. Sources with extended structures are observed less often than point-like sources. Astronomical schedules have less sources, but they are observed more intensively during an experiment and sources with extended structures are preferably picked.

We want to answer the following questions in this paper: 1) what are the metrics of geodetic parameters derived from the MOJAVE-5 dataset? 2) how worse or better these metrics are with respect to similar geodetic programs? 3) what is the main cause of these differences? And finally, we want to learn whether we can use MOJAVE-5 dataset as a testbed for investigation of the impact of source structure on geodetic and astrometric results.

3 Data analysis

The VLBA network consists of ten 25-meters radio telescopes located on the U.S. territory (eight in North America, one in the Pacific, and one in the Caribbean), see Fig. 1. The interferometric visibility data of MOJAVE-5 campaign (observing code bl229) at 15.3 GHz (Ku band) with dual circular polarization are publicly available through the National Radio Astronomy Observatory (NRAO) Science Data archive¹ in the FITS-IDI (Interferometry Data Interchange) format. We processed 33 MOJAVE-5 experiments since September 26, 2016 through July 02, 2020. The first 25 experiments (bl229aa-ay) were observed at independently recorded eight intermediate frequencies of 32 MHz width per polarization using the polyphase filter bank (PFB) personality of the digital backend. Since July 2019 (experiment bl229az) the bandwidth of a sub-band has increased to 64 MHz, which built four sub-bands covering 128 channels and MOJAVE-5 campaign has used four IFs of 64 MHz width per polarization using the direct digital converter (DDC) personality of the digital backend. In both cases the total recorded bandwidth per polarization is 256 MHz (see Table 1).

¹ <https://archive.nrao.edu/archive>

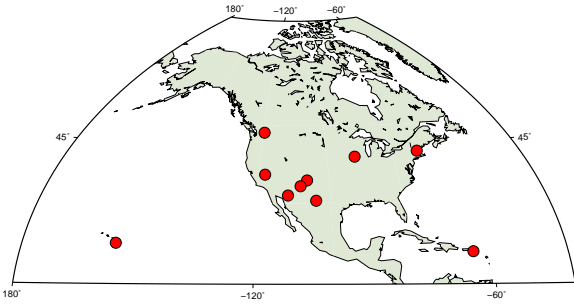


Fig. 1 Distribution of the ten VLBA radio telescopes.

Table 1 Lower edge frequency of the sub-bands in the MOJAVE-5 bl229 experiments in GHz.

bl229aa-ay	bl229az-bg
15.22400	15.17575
15.25600	15.25575
15.28800	15.31975
15.32000	15.38375
15.35200	
15.38400	
15.41600	
15.44800	

We processed the observations with the fringe-fitting software PIMA (Petrov et al., 2011) running coarse fringe fitting – bandpass calibration – fine fringe fitting and producing the output databases that include group delays and their uncertainties among other parameters. These quantities serve as input for the data analysis software package pSolve² and VieVS (Böhm et al., 2018).

As a reference dataset, we analyzed 28 geodetic RV (Regular geodesy with VLBI) (Petrov et al., 2009) and 6 CN sessions observed simultaneously at 2.3/8.6 GHz (S/X bands) for the same time span starting with rv119 on September 14, 2016 through July 07, 2020. The RV network consists of ten VLBA stations plus up to seven other geodetic stations. These sessions are designed to provide accurate estimates of the Earth orientation parameters (EOP), a highly accurate terrestrial reference frame (TRF) determination, and source position estimation where the VLBA stations are incorporated into the VLBI reference frame through the inclusion of other geodetic stations with long history of observations. In CN experiments only ten VLBA stations participate (Thomas and MacMillan, 2020).

To assess the quality of geodetic results, we estimated baseline lengths and EOP and computed their weighted root mean squares (wrms) from the astrophysics MOJAVE-5 program and dedicated geodetic

RV&CN experiments. As an extra check, we analyzed the VLBA data in several ways. One solution was produced using the software PIMA for the fringe-fitting and pSolve for the analysis. In the second solution we analyzed group delays produced with PIMA with the geodetic VLBI analysis software VieVS. For the RV&CN experiments we run another solution with VieVS where we used group delays evaluated with Fourfit visibility analysis software (Cappallo, 2017). These data products in vgosDB format were retrieved from the International VLBI Service for Geodesy & Astrometry (IVS) data archive³. Tables 2 and 3 contain the parameterization of the solutions in pSolve and VieVS, respectively. Table 4 shows weighted rms of postfit residuals. The MOJAVE-5 and RV&CN experiments are processed in the same manner with the same parameterization to allow an informative comparison.

Baseline length repeatability. We ran several solutions and we compared the scatter in baseline length estimates. We show in Fig. 2 the wrms of the estimated baseline lengths from solutions computed with pSolve (left panel) and with VieVS (right panel). Red crosses denote the baselines determined from the MOJAVE-5 experiments in both plots. We show in the left plot of Fig. 2 the baseline scatter computed from the RV&CN sessions with the whole scheduled network (blue x-signs) and with observations conducted at the VLBA stations only (green diamonds). The plot demonstrates that dropping the data obtained with non-VLBA stations does not change the wrms of the baseline lengths between the VLBA telescopes. In the right plot of that figure we compare the MOJAVE-5 bl229 baseline scatter with RV&CN sessions processed with Fourfit. We got approximately the same baseline length scatter from MOJAVE-5 and RV&CN sessions using independent software packages.

There is an increase in the baseline length repeatability from a solution using the MOJAVE-5 dataset with respect to the reference RV&CN sessions. The baseline length repeatability differences derived from RV&CN and MOJAVE-5 are about 1.3 mm at a 1000 km long baseline and 3.2 mm at the 8611 km baseline length. The coefficients of the linear regression are summarized in Table 5. We conclude the baseline length repeatability derived from analysis of single-band 15 GHz MOJAVE-5 experiments is approximately a factor of 1.5 greater than derived from the contemporary dual-band 2.3/8.6 GHz dataset.

Earth orientation parameters The Earth orientation parameters were estimated in a so-called backward solu-

² <http://astrogeo.org/psolve>

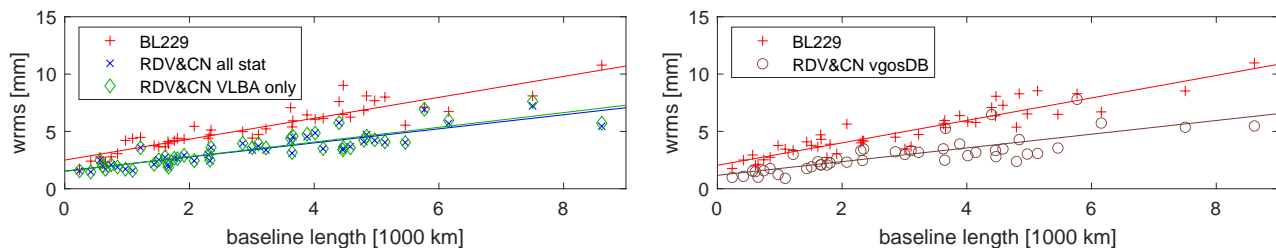
³ Available at <https://ivscc.gsfc.nasa.gov/products-data>

Table 2 Parameterization of estimated parameters of a single session solutions in pSolve.

pSolve	
CRF	selected sources
TRF	NNT/NNR condition on VLBA stations with 0.1 mm constraints
ERP	offset and rate
celestial pole offsets	offset without constraints
zenith wet delay	B-spline with time span 20 min and sigma of constraints 50 ps/h
tropo. gradients	8 hours with sigma of constr. 0.5 mm on offset and 2.00 mm/day on rate
clocks	B-spline with time span 60 min and constraint sigma 5.e-14 s/s
baseline clock offsets	offset with constraint sigma 500 ns
weights	yes

Table 3 Parameterization of estimated parameters of a single session solutions in VieVS.

VieVS	
CRF	selected sources
TRF	NNT/NNR condition on VLBA stations
ERP	pwlo with time interval 24 hours with relative constraints 1 mas
celestial pole offsets	pwlo with time interval 24 hours with relative constraints 0.1 μ as
zenith wet delay	pwlo with time interval 30 min with relative constraints 1.5 cm
tropo. gradients	pwlo with time interval 180 min with relative constraints 0.5 cm
clocks	pwlo with time interval 60 min with relative constraints 1.3 cm, one rate and quadratic term
baseline clock offsets	offset without constraints
weights	baseline-dependent weighting

**Fig. 2** Baseline length repeatability at the VLBA network. Left panel compares baseline scatter computed with pSolve from MOJAVE-5 dataset (red crosses), RV&CN dataset after processing data from all stations (blue x-signs), and RV&CN dataset when non-VLBA observations were dropped (green-diamonds). Right panel shows baseline length repeatability computed with VieVS from MOJAVE-5 dataset (red crosses) and RV&CN dataset processed with Fourfit (brown circles).**Table 4** Weighted rms of post fit residuals in ps.

	min	max	median
MOJAVE-5 bl229 series	11.3	28.7	18.4
geodetic RV&CN all stat	14.7	40.3	25.2
geodetic RV&CN VLBA only	14.7	37.8	24.1

Table 5 Parameters of the fitted linear regression model of baseline length repeatability in a form of $a \cdot L + b$ where L is length of baseline in mm.

dataset	software	a [ppb]	b [mm]
MOJAVE bl229	PIMA, pSolve	0.91	2.50
RV&CN VLBA only	PIMA, pSolve	0.64	1.51
RV&CN all stat	PIMA, pSolve	0.61	1.54
MOJAVE bl229	PIMA, VieVS	0.98	2.04
RV&CN all stat	Fourfit, VieVS	0.60	1.17

tion, i.e. in a solution consistent with globally estimated terrestrial and celestial reference frames from the processed sessions. The orientation and the origin of the TRF is set to have no-net-translation (NNT) and no-net-rotation (NNR) with respect to the ITRF2014 (Altamimi et al., 2016) for positions of all ten VLBA stations, and the CRF is oriented by imposing the no-net-rotation condition with respect to ICRF3 (Charlot et al., 2020) coordinates of defining sources. We ran several solutions similar to those we introduced in the previous paragraph and we computed the EOP using both software packages pSolve and VieVS. Table 6 shows the wrms of the ERP (polar motion components and dUT1) w.r.t. IERS 14 C04 time series after a trend and bias removal, whereas the wrms of the nutation offsets is given w.r.t. a harmonic expansion heo_20200606.heo produced from analysis of available geodetic VLBI data

since 1980 through 2020 using the method presented in Petrov (2007). In addition, the median formal error for all five EOP is summarized in the table. We show three solutions computed with pSolve similar to those introduced by the baseline length repeatability, i.e. EOP from MOJAVE-5 dataset, EOP from RV&CN sessions including all stations, and EOP from RV&CN sessions using the VLBA telescopes only. Estimation of EOP using single band observations at high frequencies was made in the past (e.g., Petrov et al., 2011). Our recent processing of 37 VLBA experiments at 24 GHz (Krásná et al., 2019) showed that although formal uncertainties were on par with dual-band regular geodetic experiments (60 μas for x-pole, 80 μas for y-pole and 5 μs for UT1), the wrms of the difference with respect to the IERS 14 C04 time series taken as a reference were greater than formal uncertainties by a factor of three for polar motion and a factor of ten for UT1. Table 6 shows that ERP determined from MOJAVE-5 data have the wrms differences with respect to the reference IERS C04 14 by a factor of 1.3 to 1.8 larger than from RV&CN experiments at the same network.

4 Differences between MOJAVE-5 bl229 and RV&CN

We recognize there are three major differences between the datasets which may have an impact on geodetic results. First, different scheduling approaches were used due to different goals of the experiments. Second, modeling of the ionospheric path delay was different since MOJAVE-5 was observed at a single-band. Third, different radio sources were selected for observations. We isolate these factors and determine which factor has the greatest impact on the accuracy of geodetic solutions.

4.1 Scheduling

Scheduling of a VLBI experiment is a complex task. The scheduler has to evaluate several criteria which lead to the best schedule according to the focus of the current experiment.

The major criteria for design of the geodetic schedule are the sky coverage over the individual stations, number of observations, and scan duration. The general scheduling concept of the established software sked for the geodetic sessions can be found in Gipson (2010). Evenly distributed observations over all elevation angles at a given station ensure a good decorrelation of station dependent parameters such as station height, zenith wet delay, clock parameters, or baseline clock offsets (e.g., Nothnagel et al. (2002)), and therefore, such schedule

can be regarded as station-centric. A large number of observations in general improves the accuracy of the estimated geodetic parameters due to higher redundancy. The challenge for the scheduling software is to find the best compromise between a) the long antenna slew time needed for the best sky coverage in a short interval (1-3 hours) allowing a high time resolution of the estimated parameters and b) the short antenna slew time allowing for a high number of observations with sufficient scan duration and high signal to noise ratio. The newly developed scheduling software VieSched++ (Schartner and Böhm, 2019, 2020) written in modern C++ which is a successor of a Matlab based VieVS scheduler (Sun, 2013; Sun et al., 2014) provides sophisticated optimization criteria and allows to create and select schedules based on simulations of the proposed observations. Recently, a new geodetic scheduling approach inspired by evolutionary processes was presented by Schartner et al. (2021) which enables the generation of fully automated and individually optimized schedules providing up to 10% more observations compared to previous scheduling approaches.

Astronomic VLBI schedules are mainly scheduled using Sched (Walker, 2020). The primary goal of the MOJAVE-5 bl229 experiments is to provide best images of jets in active galactic nuclei. Therefore, their schedule is optimized to track a small set of sources (30) in a 24-hour session in ten scans per source for a total on-source time of ~ 35 minutes. A given source is scheduled to have at least 6 antennas above 10° elevation⁴. Such schedule is considered as source-centric.

In Fig. 3 we show the sky coverage during a 24-hour observing session at three selected telescopes (BR-VLBA, FD-VLBA, SC-VLBA) where colors depict the time passed since the session start. As an example, we show the sky coverage during the MOJAVE-5 session bl229bc observed on December 22, 2019 in the upper plots and the cn1924 session observed with the same network on December 09, 2019 in the lower plots. Table 7 summarizes the mean number of scans in a 24-hour experiment at each of the ten VLBA telescopes computed over the investigated time period (September 2016 — July 2020). We see that twice as many scans at each telescope were observed in geodetic experiments with short integration time than in MOJAVE-5 observing sessions that used longer integrations. Fig. 4 presents the total number of observed sources in each session (upper plot) and the median number of observations during a 24-hour session for each source computed over the respective four years period. The median number of observed radio sources is 30 in MOJAVE-5 sessions, and 78 in RV&CN sessions. Comparison of the number

⁴ <http://www.physics.purdue.edu/astro/MOJAVE/data.html>

Table 6 Wrms and median formal error statistics of the estimated EOP from MOJAVE-5 bl229 and RV&CN series. The values for ERP are given w.r.t. IERS 14 C04 time series after trend and bias removal. The celestial pole offsets differences dX and dY were computed with respect to the empirical harmonic expansion heo_20200606.heo.

		x-pole [μas]	y-pole [μas]	dUT1 [μs]	dX [μas]	dY [μas]
MOJAVE bl229	wrms	228	286	23	169	128
	median formal error	109	153	9	59	56
RV&CN VLBA only	wrms	126	218	15	89	129
	median formal error	80	120	6	92	69
RV&CN all stat	wrms	117	130	14	72	87
	median formal error	57	89	4	86	60

Table 7 Mean number of scans at VLBA telescopes in one session computed over the period of interest (September 2016 - July 2020).

	Br	Fd	Hn	Kp	La	Mk	Nl	Ov	Pt	Sc
MOJAVE bl229 series	245	245	241	248	251	204	251	252	235	219
geodetic RV&CN experiments	451	485	445	493	483	357	467	487	451	423

of observations for each source during a whole session shows that 95% of the AGNs observed in MOJAVE-5 sessions have more than 150 observations, whereas only 35% of the sources were observed in RV&CN that often. It approves that geodetic schedules are designed to provide a good sky coverage for each station and the sources are picked up to improve the azimuth/elevation coverage regardless of how often they are observed in a given experiment.

4.2 Ionosphere

The ionosphere is a refractive media. Propagating in the ionosphere, phase delay decreases and group delay τ_{gr} increases with respect to the ionosphere free τ_{if} group delay in the absence of the ionosphere as

$$\tau_{gr} = \tau_{if} + \kappa \Delta\text{TEC} / f_{\text{eff}}^2, \quad (1)$$

where f_{eff} is the effective frequency that is within several percent of the recorded central sky frequency, ΔTEC is the differential Total Electron Content measured in TEC units (TECU, 1 TECU = 10^{16} electron/ m^2):

$$\Delta\text{TEC} = \int N_v ds_1 - \int N_v ds_2 \quad (2)$$

with s_1 and s_2 as paths of wave propagation from a source to the first and second station of the radio interferometer, and

$$\kappa = 10^{-16} \cdot \frac{e^2}{2c m_e \epsilon_o} = 5.308018 \cdot 10^{10} \text{ s}^{-1} \quad (3)$$

where e — charge of an electron, m_e — mass of an electron, ϵ_o — permittivity of free space, c — velocity of light in vacuum.

To mitigate the impact of the ionosphere on group delay, geodetic observations are usually conducted at two frequencies simultaneously. Combining group delays τ_u and τ_l at the upper and lower frequencies f_u and f_l respectively, we can derive the differential TEC and the ionosphere free path delay as

$$\begin{aligned} \Delta\text{TEC} &= \frac{f_u^2 f_l^2}{f_u^2 - f_l^2} (\tau_l - \tau_u), \\ \tau_{if} &= \frac{f_u^2}{f_u^2 - f_l^2} \tau_u - \frac{f_l^2}{f_u^2 - f_l^2} \tau_l, \\ \tau_{iu} &= \frac{f_l^2}{f_u^2 - f_l^2} (\tau_l - \tau_u). \end{aligned} \quad (4)$$

Derivations of these equations can be found for example in Petrov et al. (2011). This approach allows to effectively cancel the ionospheric contribution, leaving residual contribution at a level not exceeding several picoseconds (Hawarey et al., 2005).

MOJAVE-5 program used only one frequency. An alternative approach for modeling the ionospheric contribution is to use TEC maps from GNSS observation processing. Applying time and spacial interpolation, we can compute TEC in the vertical direction for each station and each observation. Then we can relate the TEC in the direction of observation at the elevation angle E to the TEC in the vertical direction via a mapping function $M_i(E)$. Considering the ionosphere as a thin shell at height H , we can easily derive the ionospheric

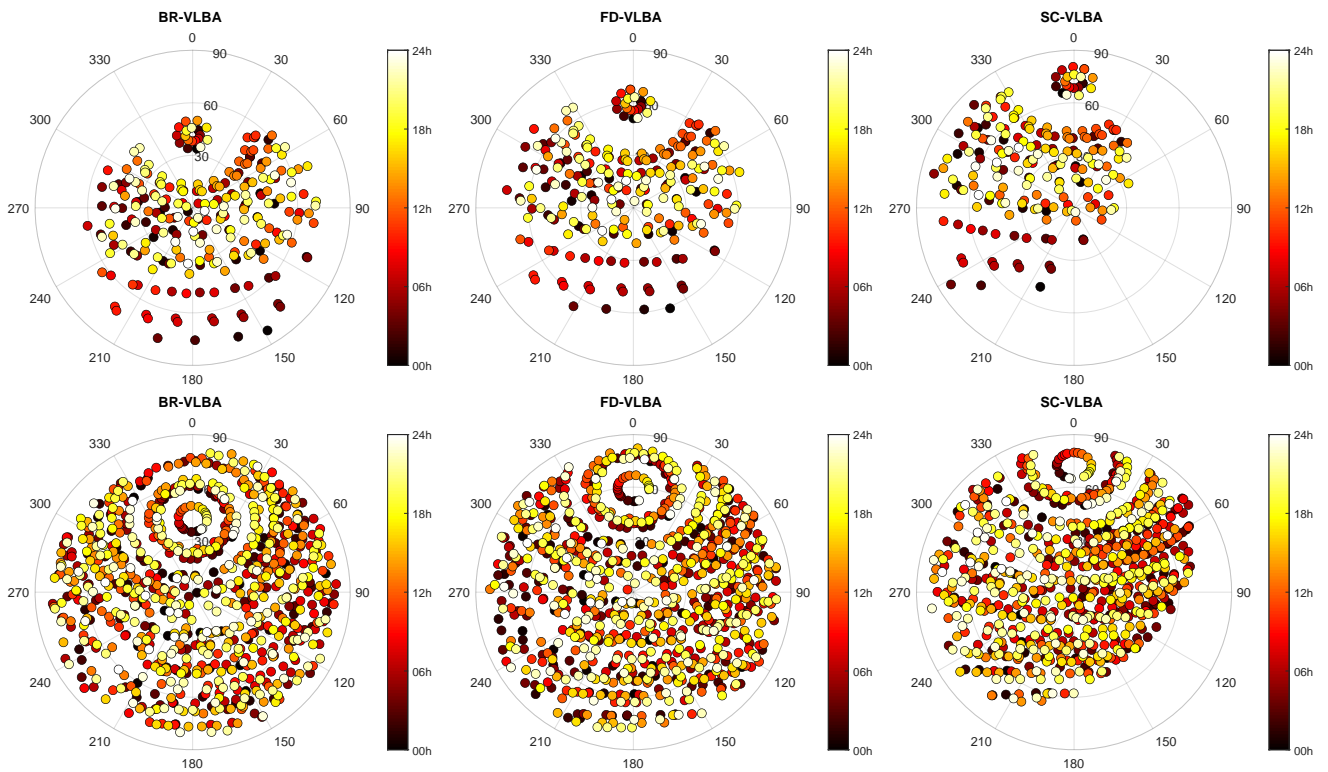


Fig. 3 Sky coverage of three VLBA stations: BR-VLBA, FD-VLBA and SC-VLBA during the bl229bc MOJAVE-5 experiment (upper plots) and the cn1924 experiment (lower plots).

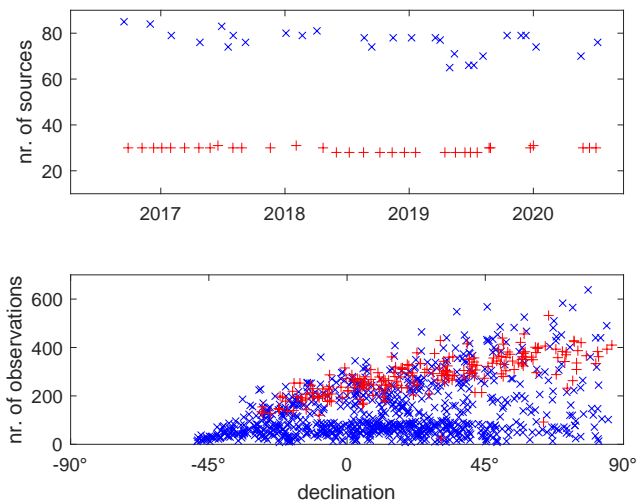


Fig. 4 The upper plot shows number of observed sources in each session. The lower plot depicts the median number of observations for each source. The red crosses stand for the bl229 experiments, blue x-signs for the RV&CN experiments.

mapping function as

$$M_i(E) = \frac{1}{\cos \beta(E)},$$

$$\beta(E) = \arcsin \frac{\cos E}{1 + \frac{H}{R_\oplus}}, \quad (5)$$

where R_\oplus is the Earth's radius.

We used Center for Orbit Determination in Europe (CODE) TEC time series (Schaer, 1999)⁵ with a resolution of $5^\circ \times 2.5^\circ \times 2^h$. This resolution is relatively coarse and accounts only for a part of the signal. Therefore, our results of processing MOJAVE-5 observations are affected by systematic errors caused by the residual ionosphere.

In order to quantify the residual ionospheric signal, we processed dual-band RV&CN data set. For the purpose of this study, we consider that the ionospheric free linear combination of X and S band group delays has no ionospheric contribution. We can form the differences between the ionospheric contribution computed from TEC maps and from X and S band group delays and investigate the properties of this stochastic process.

Solving for zenith path delay in the neutral atmosphere will pick up a portion of the slowly varying bias, but the ionospheric fluctuations at scales less than several hours will propagate to residuals. Though, we can characterize stochastic properties of the residual signal similar to the approaches developed in Petrov et al. (2011, 2019); Petrov (2021). The ionospheric path delay fluctuation is a non-stationary process. We can expect that fluctuations at scales x will be related to fluctua-

⁵ Available at <ftp://ftp.aiub.unibe.ch/CODE>

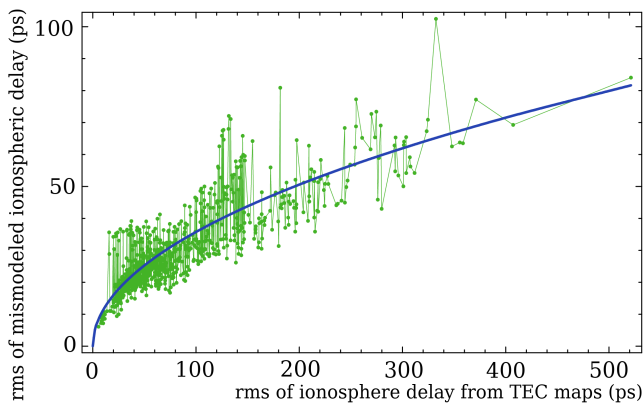


Fig. 5 The rms of the errors in the ionospheric path delay as a function of the rms of the variations of the ionospheric group delays derived from TEC maps (green dots). The solid blue line shows a regression in a form of the power law $1/2$.

tions at scales y via a power law from the general results of the turbulence theory. Therefore, we did the following:

First, we computed the mean differences of $d_{gv} = \tau_{ig} - \tau_{iv}$ between the ionospheric path delay at X band computed from TEC maps (τ_{ig}) and from VLBI dual band observables (τ_{iv}) for every baseline and every experiment in the RV&CN dual-band dataset, and then we subtracted the mean value from d_{gv} . The mean value is the sum of the bias between TEC maps and VLBI ionospheric path delay and a constant instrumental delay in VLBI hardware. Since the constant instrumental delay that may be even greater than the ionospheric signal is not calibrated, the mean value of d_{gv} is meaningless. Then we computed the rms over d_{gv} . We discarded the data with clock jumps that may happen at only one band. We got time series of $\text{rms}(d_{gv})$ and we examined empirical relationships of $\text{rms}(d_{gv})$ with other statistics. We found that $\text{rms}^2(d_{gv})$ has a linear dependence on $\text{rms}(\tau_{ig})$. The power law dependence between d_{gv} and τ_{ig} was expected, but the power law coefficient, 2, is purely empirical. Fig. 5 demonstrates the time series of d_{gv} and their fit.

We can compute the rms of the ionospheric errors at a given baseline of a given experiment via

$$\text{rms}(d_{gv}) = \sqrt{\rho \text{rms}(\tau_{ig})}, \quad (6)$$

where ρ is the empirical coefficient determined from fitting (see Fig. 5) equal to 12.8 ps and the rms is expressed in ps. This empirical relationship allows us to predict the second moment of the residual noise after we perform data reduction for the ionospheric contribution using TEC maps. One can expect that if the TEC variance is greater, the residual errors are also greater. Expression (6) quantifies this dependence.

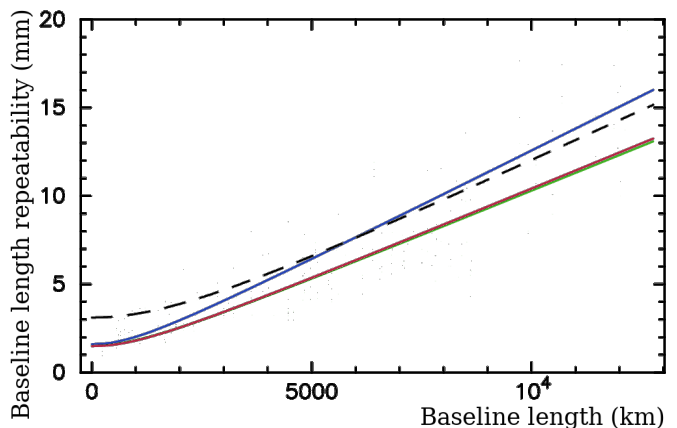


Fig. 6 The dependencies of the baseline length repeatability fits on the baseline length. The upper blue curve shows the baseline repeatability for the X band only in the “bx” solution that uses GNSS TEC maps. Two lower very close curves, red and green, show the baseline length repeatability for the “bu” solution that demonstrates the effect of mismodeled ionosphere on Ku band observable, and the reference dual band solution. The dashed black line shows the baseline length repeatability from the MOJAVE-5 solution.

We have computed baseline-dependent additive noise due to mismodeled ionosphere for every baseline and every experiment of MOJAVE-5 program using τ_{ig} . We added that noise to the a priori group delay errors in quadrature and computed new weights. We ran several baseline solutions, computed baseline repeatabilities, and compared them with the reference dual-band solution using RV&CN data. In solution “bx” we used the ionosphere-free combinations of group delays, added the contribution of the ionosphere τ_{iu} to them, and processed these data the same way as MOJAVE-5 data, i.e. performing data reduction for the ionosphere using CODE TEC maps and inflating a priori group delay uncertainties for the additional noise due to mismodeling the ionosphere. In the second solution “bu” we simulated how the deficiency of CODE TEC model would have impacted our RV&CN solution, as if these experiments ran at 15.3 GHz instead of 2.3/8.6 GHz. To achieve this, we re-scaled τ_{iu} by the square of the frequency ratio $(8.64/15.28)^2 \approx 0.32$. Fig. 6 shows fit in a form $\sqrt{(aL)^2 + b^2}$ for all these solutions. The baseline length repeatability from MOJAVE-5 solution is shown by the dashed line.

We found that the impact of the mismodeling ionosphere on the baseline length repeatability of VLBA data collected in 2016–2020 at 15.3 GHz during Solar minimum is negligible. Therefore, an increase in the baseline length repeatability from a geodetic solution using the MOJAVE-5 dataset with respect to the reference dual-band RV&CN solution cannot be explained by the unaccounted contribution of the ionosphere. We

should caution that this result should not be extrapolated to other estimated parameter, such as source position, and should not be extrapolated to epochs of the Solar maximum.

4.3 Simulations

To touch the effect of source structure, we run simulations of the observations. Using the simulation VieVS tool (Pany et al., 2011), we replaced group delay observables with synthetic artificial group delays provided by the random noise generator as

$$\tau_{gr} = \tau_{mod} + (\tau_{clk} + \tau_{zwd} + \tau_{fl}). \quad (7)$$

We add three stochastic error sources to the theoretically computed time delay (τ_{mod}): delay caused by the turbulence in the troposphere (τ_{zwd}), station clock (τ_{clk}), and the Gaussian noise (τ_{fl}) with $\sigma=20$ ps that accounts for the thermal noise and instrumental errors. We used the model of Nilsson et al. (2007) for simulation of zenith wet delay implemented in VieVS. In the framework of that approach we consider that the atmospheric turbulence for every station is described with a structure function with the refractive index structure constant $C_n = 1.8 \cdot 10^{-7} \text{ m}^{-1/3}$, the effective height $H = 2$ km, and the constant wind velocity $v = 8$ m/s towards East. Then we computed the covariance matrix between group delays for each pair of observations of a given station and used them for computation of the full weight matrices under an assumption that the atmospheric turbulence is a stationary process. The simulation of station clocks was performed with an Allan standard deviation of $1 \cdot 10^{-14}$ at 50 min. We did not include modeling source structure into simulation.

We have computed baseline length repeatabilities from simulated RV&CN and MOJAVE-5 datasets. The regression lines in a form $a \cdot L + b$ for simulated and real data are shown in Fig. 7. We see from these plots that simulation results show even deeper disparity in repeatabilities between MOJAVE-5 and RV&CN data as we saw in real observations. We should note that τ_{clk} and τ_{fl} in equation (7) are exactly the same for both datasets, and τ_{zwd} that is dependent on elevations and time is similar in both datasets because it is derived from the same model. Therefore, the stochastic model we used for MOJAVE-5 and RV&CN simulations is essentially the same. This finding pinpoints the origin of discrepancies in results of processing real data: differences in schedules.

Since atmospheric path delay and clock function are modeled in a form of an expansion over the B-spline basis with a time span 20–60 minutes, in order to decorrelate these two groups of nuisance parameters and the

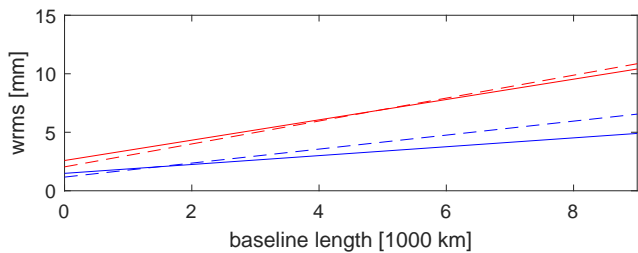


Fig. 7 The wrms of baseline length from simulated (dashed line) and real observations (solid line). The upper red lines show the baseline length repeatability from analysis and simulation of MOJAVE-5 data. The low blue lines shows results of analysis and simulation of RV&CN data.

Table 8 The wrms of the simulated EOP from MOJAVE-5 bl229 and RV&CN experiments observed at the VLBA network. The wrms statistics of the differences between EOP estimates the IERS 14 C04 time series after trend and bias removal are shown below.

	x-pole [μas]	y-pole [μas]	dUT1 [μs]	dX [μas]	dY [μas]
MOJAVE-5 bl229	158	225	16	82	98
RV&CN VLBA only	118	184	10	82	97

station vertical component, observations at significantly different elevations are required. Fig. 8 shows that the spread of observations over mapping function (approximately reciprocal to sine of elevation angle which equals to the partial derivative of the time delay w.r.t. zenith wet delay) for geodetic experiment rv119 is noticeably wider and observations at elevations below 30° , which corresponds to mapping function > 2 , are much more often than in astronomical experiment bl229aa.

In order to look at the problem deeper, we investigated correlations between estimates of the vertical site position and atmospheric path delays. The median correlation coefficient is -0.22 for RV&CN sessions and -0.35 for MOJAVE-5 sessions computed from the real data. We ran a series of solutions using RV&CN data and flagged out observations below a certain elevation angle. Table 9 summarizes the findings. An increase of the elevation cutoff results in an increase of the baseline length repeatability. MOJAVE-5 has few scans below elevations 30° and none below 20° . The achieved baseline length repeatability from MOJAVE-5 experiments is similar to the repeatability from RV&CN experiments when observations below 20 – 25° are not included in a solution. Fig. 9 shows individual correlation coefficients in simulated geodetic experiment cn1924 for cutoff elevation 3° , 20° and 30° . The median correlation coefficient between vertical displacement and clock offset at the respective station is 0.19, 0.27 and 0.39 for the increasing cutoff elevation angle. The median cor-

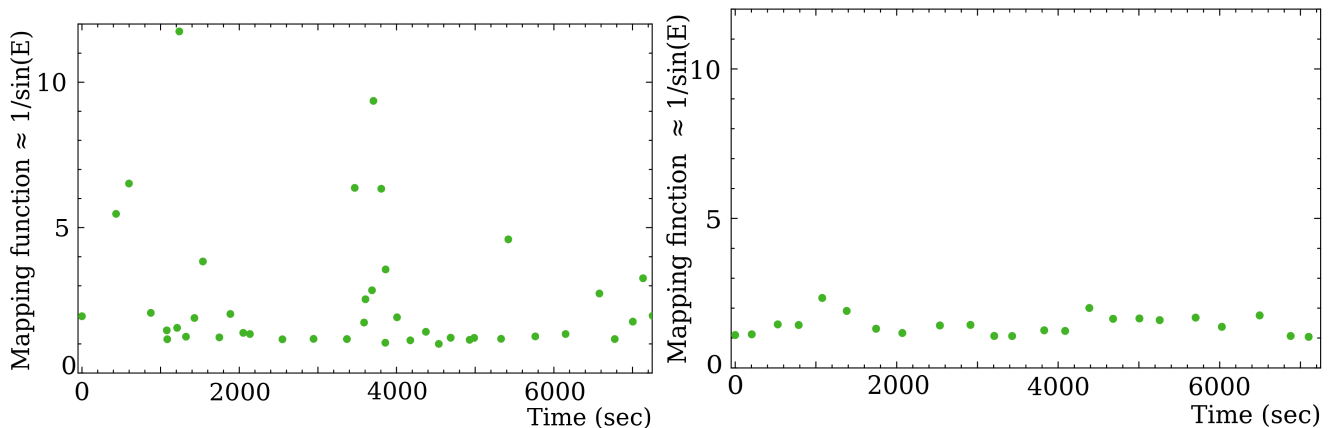


Fig. 8 The distribution of observations over the mapping function for station LA-VLBA within first two hours of an experiment. Since deviation of the mapping function from $1/\sin(\text{elevation})$ is small at elevations above 10 deg, mapping function $1/\sin(\text{elevation})$ is used here for illustrative purpose. *Left*: geodetic experiment rv119. *Right*: astronomical experiment bl229aa.

Table 9 The coefficients of the baseline length repeatability regression in a form of $a \cdot L + b$ as a function of elevation angle from processing RV&CN VLBA observations.

Elevation cutoff	a [ppb]	b [mm]
0°	0.55	1.46
5°	0.55	1.46
10°	0.70	1.35
15°	0.90	1.14
20°	1.09	1.14
25°	1.22	1.14
30°	1.86	1.49

relation coefficient between vertical component and a residual atmospheric zenith path delay is -0.37, -0.64 and -0.79 when the elevation cutoff is increasing. This proves that strategy including radio sources under low elevations in the schedule over short periods of time allows to decorrelate station dependent parameters in the data analysis and to provide better baseline length repeatability.

We also investigated the residual EOP estimates from the simulated RV&CN and MOJAVE-5 datasets with respect to the IERS C04 14 time series taken as a reference. The results of this simulation are presented in Table 8. The simulation results confirm about the same disparity of 20-60% of the wrms from MOJAVE-5 and RV&CN dataset as in the results derived from real observations (compare with Table 6).

4.4 Insight on the possible contribution of the source structure

The first indicator of astrometric source quality based on source structure corrections was developed by Fey and Charlot (1997). They derived the so-called structure index (SI) from VLBI source images as the median

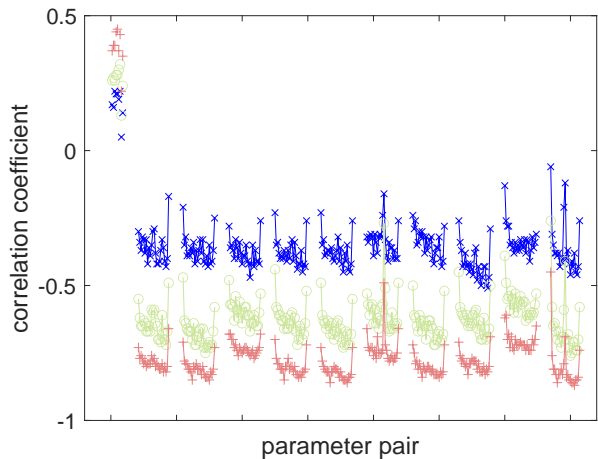


Fig. 9 Correlation coefficients in simulated geodetic experiment cn1924 for cutoff elevation 3° (blue x-signs), 20° (green circles) and 30° (pink crosses). The order of parameter pairs at the x axis: (1st–9th): station’s vertical component and clock offset for all stations except of the clock reference; (10th–last): station’s vertical component and a residual atmospheric zenith path delay (estimated as pwlo every hour) for all ten stations (the solid line connects coefficients which belong to the same station).

value of the group structure delay (τ_{str}) determined for pixels in a 512×512 uv -grid for all baselines less than the diameter of the Earth. Fig. 10 shows images of the three most observed sources in bl229aa (0636+680, 0210+515 and 0128+554) and in rv119 (2229+695, 0345+460, 0529+483) which are the first sessions of our datasets. We computed the SI for all sources observed in bl229aa. For that calculation we used maps provided by MOJAVE team⁶ and split the sources in the four SI groups according to the median value of calculated structure

⁶ Available at <https://www.physics.purdue.edu/MOJAVE>

delay corrections. Among 30 sources observed in bl229aa, 3 sources have SI 1, 14 sources SI 2, 8 sources SI 3, and 5 sources have the highest SI 4. Fig. 11 shows post fit residuals in session bl229aa for real observations v_{real} (lower plots) and for simulated observations v_{sim} (upper plots). As an example, we highlight the most observed source 0636+680 in this session which has structure index 2 and 0128+554 with structure index 4. The comparison shows that the scatter of delay residuals for 0636+680 is similar to real and simulated observations and the rms reaches 29.6 ps and 29.3 ps, respectively. The rms of delay residuals from source 0128+554 with extended structure is 2.5 times larger from real observations compared to the simulated ones, i.e. 72.3 ps and 27.4 ps, respectively. We computed the rms of delay residuals for every source in the bl229aa experiment and built the difference between the rms from real and simulated observations. The median value of the rms difference was calculated as

$$\Delta\text{rms}_{\text{med}} = \text{med}(\text{rms}(v_{real}) - \text{rms}(v_{sim})) \quad (8)$$

over each source group with respect to the structure index. The obtained median values are summarized in Table 10. We see that the difference between simulated and real delay residuals is raising with an increasing source structure index since the structure group delay is not modeled in the simulated observations. With the SI 1 taken as reference, the rms of the delay residuals increases by about 36 ps for sources with SI 4. The lower wrms of postfit residuals from processing real observations compared to the simulated ones for sources with low structure indices (SI 1 and SI 2) that is manifested by the negative $\Delta\text{rms}_{\text{med}}$ is due to the fact that the excessive noise due to source structure is less than the random Gaussian noise with the rms of 20 ps that had been added to simulated path delay in our simulation.

We see that the source structure contribution increases the rms of the postfit residuals but such an increase even for a subset of sources with strong radio jets picked up for an astronomical program does not have a noticeable impact on baseline length repeatability. Source structure causes not only random but also systematic errors, but their impact on the baseline length repeatability is insignificant. We exercise a caution to extrapolate this result to source position estimates. This requires a further investigation that is beyond the scope of present work.

5 Conclusions

We have processed 33 diurnal astronomical observing VLBI sessions at 15 GHz under program MOJAVE-5 and 28 diurnal VLBI geodetic dual-band observing

Table 10 Median of rms differences $\Delta\text{rms}_{\text{med}}$ between delay residuals from real and simulated observations in bl229aa. Sources are divided in four groups according to their structure index, i.e. according to their median group structure delay $\text{med}(\tau_{\text{str}})$. N_{sou} stands for number of sources in the group.

SI	$\text{med}(\tau_{\text{str}})$ [ps]	N_{sou}	$\Delta\text{rms}_{\text{med}}$ [ps]
1	0 – 3	3	-11.3
2	3 – 10	14	-6.6
3	10 – 30	8	9.0
4	30 – ∞	5	25.0

sessions at 2 and 8 GHz under programs RV and CN. Both observing sessions ran at the same ten station VLBA network with baseline lengths in a range from 237 to 8612 km at approximately the same time interval 2016.7–2020.5.

We found that while the wrms of post-fit residuals from MOJAVE-5 program was lower than from RV&CN, 16.37 ps versus 26.13 ps, important metrics of the geodetic quality of solutions, such as baseline length repeatability and wrms of the differences of the ERP with respect to the reference IERS C04 times series were a factor 1.3 to 1.8 worse. We investigated the origin of these discrepancies. We have established that modeling the ionospheric path delay using the GNSS TEC maps was adequate for processing 15 GHz data during the Solar minimum, and the errors of these TEC maps did not affect baseline length repeatability at a noticeable level. We investigated whether the source structure can be a factor, since MOJAVE-5 targeted objects with strong radio jets and we have not found evidence it affected baseline length repeatability. Finally, we ran solutions with simulated right hand sides for both MOJAVE-5 and RV&CN programs. The stochastic model used for these simulations was almost the same. We were able to reproduce discrepancies in baseline lengths and EOP time series statistics.

We have established that the major factor that causes discrepancies in baseline length repeatability is a more agile schedule of RV&CN experiments that includes more scans at low and high elevations at short time intervals 1–3 hours than astronomical experiments. We showed that the correlation coefficients between the station vertical component and atmospheric zenith path delay increase with an increasing elevation cutoff angle. When we removed observations below 20–25° elevations in RV&CN, we got a similar repeatability as in MOJAVE-5 program.

Although the use of single-band astronomical VLBI data from MOJAVE-5 program for geodesy provided less accurate results than the use of VLBI data from the dedicated geodesy RV&CN campaign, the baseline length repeatability is still below 1 ppb. This gives us

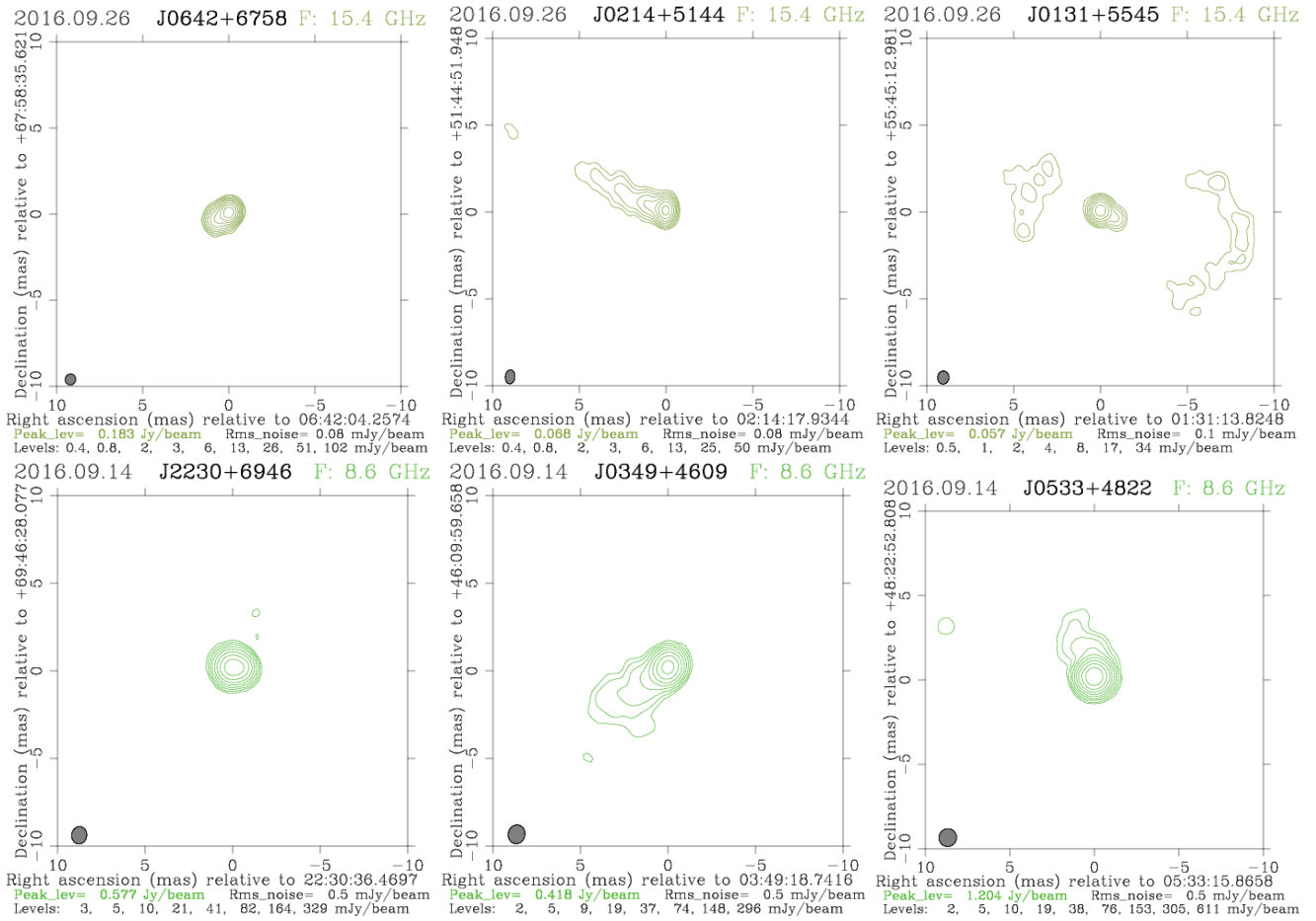


Fig. 10 Images of three most observed sources (0636+680 with SI 2, 0210+515 with SI 3 and 0128+554 with SI 4) in the bl229aa MOJAVE-5 experiment (upper plots) and in the rv119 experiment at X band (lower plots: 2229+695 with SI 2, 0345+460 with SI 2, 0529+483 with SI 2). We have produced images from rv119 ourselves. The images in FITS format are available in the Astrogate VLBI FITS image database http://astrogate.org/vlbi_images. Information about the structure index for the X band sources was taken from the Bordeaux VLBI Image Database available at <http://bvid.astrophy.u-bordeaux.fr>.

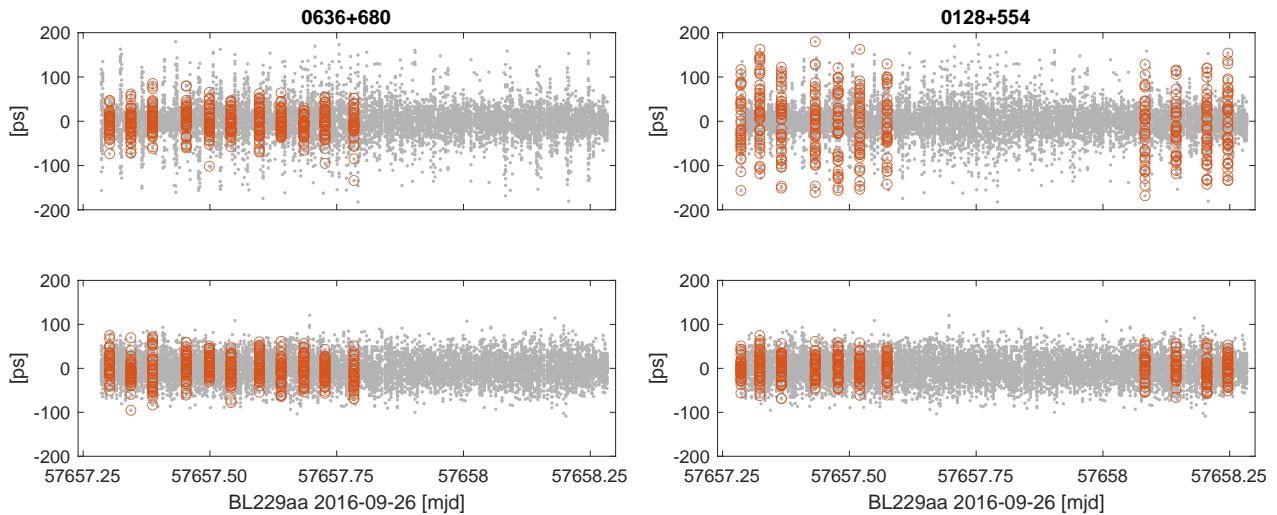


Fig. 11 Post fit residuals in session bl229aa for real (upper plots) and simulated (lower plots) observations. Highlighted are sources 0636+680 with SI 2 on the left and 0128+554 with SI 4 on the right.

a good estimate of the impact of remaining systematic errors that are specific for MOJAVE-5. This very low level of systematic errors confirms that MOJAVE-5 dataset is an excellent testbed for investigation of the effect of source structure on astrometry and geodesy in full detail.

Acknowledgements HK works within the Hertha Firnberg position T697-N29, funded by the Austrian Science Fund (FWF). LP work was supported by the NASA Earth Surface and Interior program, project 19-ESI19-0030. This research has made use of data from the MOJAVE database that is maintained by the MOJAVE team (Lister et al., 2018). The Very Long Baseline Array (VLBA) is operated by the National Radio Astronomy Observatory, which is a facility of the National Science Foundation, and operated under cooperative agreement by Associated Universities, Inc. The authors acknowledge use of the VLBA under the US Naval Observatory’s time allocation. This work supports USNO’s ongoing research into the celestial reference frame and geodesy.

References

- Altamimi Z, Rebischung P, Métivier L, Collilieux X (2016) Itrf2014: A new release of the international terrestrial reference frame modeling nonlinear station motions. *Journal of Geophysical Research: Solid Earth* 121(8):6109–6131, DOI <https://doi.org/10.1002/2016JB013098>
- Anderson JM, Xu MH (2018) Source structure and measurement noise are as important as all other residual sources in geodetic VLBI combined. *Journal of Geophysical Research: Solid Earth* 123(11):10,162–10,190, DOI <https://doi.org/10.1029/2018JB015550>
- Böhm J, Böhm S, Boisits J, Girdiuk A, Gruber J, Hellerschmied A, Krásná H, Landskron D, Madzak M, Mayer D, McCallum J, McCallum L, Schartner M, Teke K (2018) Vienna VLBI and Satellite Software (VieVS) for Geodesy and Astrometry. *Publications of the Astronomical Society of the Pacific* 130(986):044503, DOI <https://doi.org/10.1088/1538-3873/aaa22b>
- Cappallo R (2017) fourfit user’s manual, Version 1.0. https://www.haystack.mit.edu/wp-content/uploads/2020/07/docs_hops_009_fourfit_users_manual.pdf
- Charlot P, Jacobs CS, Gordon D, Lambert S, de Witt A, Böhm J, Fey AL, Heinkelmann R, Skurikhina E, Titov O, Arias EF, Bolotin S, Bourda G, Ma C, Malkin Z, Nothnagel A, Mayer D, MacMillan DS, Nilsson T, Gaume R (2020) The third realization of the international celestial reference frame by very long baseline interferometry. *Astron. & Astrophys.* 644:A159, DOI <https://doi.org/10.1051/0004-6361/202038368>
- Fey AL, Charlot P (1997) VLBA observations of radio reference frame sources. ii. astrometric suitability based on observed structure. *ApJS* 111:95–142, DOI <https://doi.org/10.1086/313017>
- Gipson J (2010) An introduction to Sked. In: Behrend D, Baver K (eds) *IVS GM Proceedings, NASA/CP 2010-215864*, pp 77–84
- Greisen EW (2003) AIPS, the VLA, and the VLBA. In: Heck A (ed) *Information Handling in Astronomy - Historical Vistas, Astrophysics and Space Science Library*, vol 285, p 109, DOI https://doi.org/10.1007/0-306-48080-8_7
- Hawarey M, Hobiger T, Schuh H (2005) Effects of the 2nd order ionospheric terms on VLBI measurements. *Geophys Res Lett* 32:L11304, DOI <https://doi.org/10.1029/2005GL022729>
- Helmholtz JF, Taylor GB, Tremblay S, Fassnacht CD, Walker RC, Myers ST, Sjouwerman LO, Pearson TJ, Readhead ACS, Weintraub L, Gehrels N, Romani RW, Healey S, Michelson PF, Blandford RD, Cotter G (2007) The VLBA imaging and polarimetry survey at 5 GHz. *Astrophys. J.* 658(1):203–216, DOI <https://doi.org/10.1086/511005>, URL <https://doi.org/10.1086%2F511005>
- Krásná H, Gordon D, de Witt A, Jacobs CS, Soja B (2019) Earth Orientation Parameters Estimated From K-band VLBA Measurements. In: Haas R, Garcia-Espada S, Lopez Fernandez J (eds) *Proceedings of the 24th European VLBI Group for Geodesy and Astrometry Working Meeting, Chalmers University of Technology*, vol 24, pp 238–242, DOI <https://doi.org/10.7419/162.08.2019>, ISBN:978-84-416-5634-5
- Lister ML, Aller MF, Aller HD, Hodge MA, Homan DC, Kovalev YY, Pushkarev AB, Savolainen T (2018) MOJAVE. XV. VLBA 15 GHz Total Intensity and Polarization Maps of 437 Parsec-scale AGN Jets from 1996 to 2017. *ApJS* 234(1):12, DOI <https://doi.org/10.3847/1538-4365/aa9c44>
- Nilsson T, Haas R, Elgered G (2007) Simulations of atmospheric path delays using turbulence models. In: Böhm J, Pany A, Schuh H (eds) *Proceedings of the 18th European VLBI Group for Geodesy and Astrometry Working Meeting, Technische Universität Wien*, pp 175–180, ISSN: 1811–8380
- Nothnagel A, Vennebush M, Campbell J (2002) On Correlations Between Parameters in Geodetic VLBI Data Analysis. In: Vandenberg NR, Baver KD (eds) *IVS GM Proceedings, NASA*, pp 260–264, NASA/CP-2002-210002

- Pany A, Böhm J, MacMillan D, Schuh H, Nilsson T, Wresnik J (2011) Monte Carlo simulations of the impact of troposphere, clock and measurement errors on the repeatability of VLBI positions. *J. Geodesy* 85:39–50, DOI <https://doi.org/10.1007/s00190-010-0415-1>
- Petrov L (2007) The empirical Earth rotation model from VLBI observations. *Astron. & Astrophys.* 467(1):359–369, DOI <https://doi.org/10.1051/0004-6361:20065091>, [astro-ph/0611781](https://arxiv.org/abs/astro-ph/0611781)
- Petrov L (2011) The Catalog of Positions of Optically Bright Extragalactic Radio Sources OBRS-1. *Astronom. J.* 142:105, DOI <https://doi.org/10.1088/0004-6256/142/4/105>, [1103.2840](https://arxiv.org/abs/1103.2840)
- Petrov L (2013) The Catalog of Positions of Optically Bright Extragalactic Radio Sources OBRS-2. *Astronom. J.* 146:5, DOI <https://doi.org/10.1088/0004-6256/146/1/5>, [1301.5407](https://arxiv.org/abs/1301.5407)
- Petrov L (2021) The Wide-field VLBA Calibrator Survey: WFCs. *Astronom. J.* 161(1):14, DOI <https://doi.org/10.3847/1538-3881/abc4e1>, [2008.09243](https://arxiv.org/abs/2008.09243)
- Petrov L, Kovalev YY (2017) Observational consequences of optical band milliarcsec-scale structure in active galactic nuclei discovered by Gaia. *Mon. Not. Roy. Astron. Soc.* 471:3775–3787, DOI <https://doi.org/10.1093/mnras/stx1747>, [1704.07365](https://arxiv.org/abs/1704.07365)
- Petrov L, Taylor GB (2011) Precise Absolute Astrometry from the VLBA Imaging and Polarimetry Survey at 5 GHz. *Astronom. J.* 142:89, DOI <https://doi.org/10.1088/0004-6256/142/3/89>, [1106.2382](https://arxiv.org/abs/1106.2382)
- Petrov L, Gordon D, Gipson J, MacMillan D, Ma C, Fomalont E, Walker RC, Carabajal C (2009) Precise geodesy with the Very Long Baseline Array. *J. Geodesy* 83:859–876, DOI <https://doi.org/10.1007/s00190-009-0304-7>, [0806.0167](https://arxiv.org/abs/0806.0167)
- Petrov L, Kovalev YY, Fomalont EB, Gordon D (2011) The Very Long Baseline Array Galactic Plane Survey—VGaPS. *Astronom. J.* 142:35, DOI <https://doi.org/10.1088/0004-6256/142/2/35>, [1101.1460](https://arxiv.org/abs/1101.1460)
- Petrov L, Kovalev YY, Fomalont EB, Gordon D (2011) The Very Long Baseline Array Galactic Plane Survey—VGaPS. *Astronom. J.* 142(2):35, DOI <https://doi.org/10.1088/0004-6256/142/2/35>
- Petrov L, Phillips C, Bertarini A, Murphy T, Sadler EM (2011) The LBA Calibrator Survey of southern compact extragalactic radio sources - LCS1. *Mon. Not. Roy. Astron. Soc.* 414:2528–2539, DOI <https://doi.org/10.1111/j.1365-2966.2011.18570.x>, [1012.2607](https://arxiv.org/abs/1012.2607)
- Petrov L, de Witt A, Sadler EM, Phillips C, Horiuchi S (2019) The Second LBA Calibrator Survey of southern compact extragalactic radio sources - LCS2. *Mon. Not. Roy. Astron. Soc.* 485(1):88–101, DOI <https://doi.org/10.1093/mnras/stz242>, [1812.02916](https://arxiv.org/abs/1812.02916)
- Schaer S (1999) Mapping and predicting the Earth's ionosphere using the Global Positioning System. *Geod-Geophys Arb Schweiz*, Vol 59, 59, <http://ftp.aiub.unibe.ch/papers/ionodiss.ps>
- Schartner M, Böhm J (2019) VieSched++: A new VLBI scheduling software for geodesy and astrometry. *Publications of the Astronomical Society of the Pacific* 131:084501, DOI <https://doi.org/10.1088/1538-3873/ab1820>
- Schartner M, Böhm J (2020) Optimizing schedules for the VLBI global observing system. *J. Geodesy* 94:1–12, DOI <https://doi.org/10.1007/s00190-019-01340-z>
- Schartner M, Plötz C, Soja B (2021) Automated VLBI scheduling using AI-based parameter optimization. *J. Geodesy* 95:58, DOI <https://doi.org/10.1007/s00190-021-01512-w>
- Shabala S, McCallum JN, Plank L, Böhm J (2015) Simulating the effects of quasar structure on parameters from geodetic VLBI. *J. Geodesy* 89:873–886, DOI <https://doi.org/10.1007/s00190-015-0820-6>
- Sovers OJ, Charlot P, Fey AL, Gordon D (2002) Structure Corrections in Modelling VLBI Delays for RDV Data. In: Vandenberg NR, Baver KD (eds) *IVS GM Proceedings*, NASA, pp 243–247, nASA/CP-2002-210002
- Sun J (2013) VLBI scheduling strategies with respect to VLBI2010. *Geowissenschaftliche Mitteilungen* 92, <https://repositum.tuwien.at/handle/20.500.12708/975>
- Sun J, Böhm J, Nilsson T, Krásná H, Böhm S, Schuh H (2014) New vlbi2010 scheduling strategies and implications on the terrestrial reference frames. *J. Geodesy* 88:449–461, DOI <https://doi.org/10.1007/s00190-014-0697-9>
- Thomas CC, MacMillan D (2020) CORE operation center report. In: Armstrong KL, Baver KD, D B (eds) *International VLBI Service for Geodesy and Astrometry 2017+2018 Biennial Report*, NASA/TP-2020-219041, pp 185–188
- Tornatore V, Charlot P (2007) The impact of radio source structure on European geodetic VLBI measurements. *J. Geodesy* 81:469–478, DOI <https://doi.org/10.1007/s00190-007-0146-0>
- Walker R (2020) The SCHED User Manual, Version 11.6. <http://www.aoc.nrao.edu/software/sched/index.html>
- Zeppenfeld G (1993) Einflüsse der Quellenstruktur in der Praxis der geodätischen VLBI. *Mitt Geod Inst Rheinischen Friedrich-Wilhelms-Univ Bonn* 80